

RESEARCH

Open Access



Use of Higher-Harmonic and Intermodulation Generation of Ultrasonic Waves to Detecting Cracks due to Steel Corrosion in Reinforced Cement Mortar

Miguel Ángel Climent-Llorca^{1*}, Marina Miró-Oca¹, Pedro Poveda-Martínez² and Jaime Ramis-Soriano²

Abstract

The aim of this work was to provide further confirmation of the possible use of non-linear ultrasonic techniques for detecting the cracking due to corrosion of steel reinforcements in concrete. To this end accelerated steel corrosion tests have been conducted on model reinforced cement mortar specimens, while monitoring the appearance and width evolution of visible surface cracks, and performing non-linear ultrasonic measurements based on the phenomena of harmonic distortion and intermodulation. A new parameter, based on the difference between the amplitude of the fundamental frequency and the sum of the amplitudes of all the first-order and second-order intermodulation products, has been proposed in this work. The results confirm that the appearance of visible surface micro-cracks are preceded and accompanied by the observation of strong non-linear features in the received signal. Furthermore, the new parameter proposed in this work is as efficient as the relative non-linearity parameters, classically used in harmonic distortion non-linear ultrasonic studies, for detecting the non-linear features associated with the critical events of the cracking of cement mortar due to embedded steel corrosion. A hypothesis has been developed considering the possible effect of the filling of the void space by liquid containing rust products after the formation of new cracks or the enlargement of its width. This filling process, which might be particularly enhanced by net convective transport of liquid, would explain the evolution of the values of all the parameters used for putting in evidence the non-linear elastic features after the critical events of the cracking process.

Keywords: reinforced concrete, steel corrosion, cracking, non-linear ultrasonic test, non-destructive detection

1 Introduction

Corrosion of steel rebar in reinforced concrete or cement mortar constructive elements is a problem of major concern in both the exploitation and maintenance of building and civil engineering structures (American Concrete Institute 1996). Usually, when this kind of structures are subjected to harmful environmental agents (e.g.,

seawater, rain, high humidity, drastic thermal changes, etc.) continuously over time, steel corrosion products are generated, which leads to stress cracking phenomena of the cementitious matrix, and the unexpected sudden failure of the structure (Bertolini et al. 2013). For this reason, the development of assessment protocols and strategies to control this problem and to prevent that fatal scenario is of great importance. Among these assessment procedures, the so-called electrochemical techniques (ASTM C876-91 1991; Elsener et al. 2003; Andrade and González 1978; Andrade et al. 2000), allow to determine some electrochemical parameters related with the development of the deterioration process. The most important of these

*Correspondence: ma.climent@ua.es

¹ Civil Engineering Department, University of Alicante, Sant Vicent del Raspeig, 03690 Alicante, Spain

Full list of author information is available at the end of the article
Journal information: ISSN 1976-0485 / eISSN 2234-1315

parameters is the corrosion rate of steel in the reinforced concrete structure, which can be used as input in theoretical models devoted to estimate its remaining service life (EHE-08 2010). Unfortunately, these techniques do not provide information about the cracks induced by the corrosion phenomena in the cementitious matrix of the composite materials.

Ultrasonic techniques are one of the most extended approaches for the detection of cracks and defects in a wide range of materials, including cementitious materials, due to its non-destructive character and straight applicability to on-site studies (Blitz and Simpson 1995). In this context, there are passive techniques for damage monitoring in concrete, based on acoustic emission phenomena (Ohtsu 2010; Zaki et al. 2015); and active ones that imply the generation and propagation of ultrasonic waves throughout the material under analysis. These active techniques use the impact-echo method (Liang and Su 2001) or the ultrasonic pulse velocity (UPV) test. Nevertheless, even though there is a standardized procedure to carry out these latter measurements (ASTM C597-16 2016), it has been shown that the sensitivity and accuracy of these linear techniques are to certain extent limited for the detection of micro-cracks compared to non-linear techniques (Jhang 2009; Shah and Ribakov 2009a; Antonaci et al. 2012, 2013). During the last years, many research efforts have been made on the development of these non-linear ultrasonic (NLU) techniques so as to increase the detection features of the tests. Some of these techniques are based on changes in the resonance frequency (spectroscopy) (Van den Abeele et al. 2000), on the generation of higher order harmonics (Shah and Ribakov 2009b), or on the emergence of intermodulation products (Burrascano et al. 2019). The appearance or increase of the amplitude of harmonics

or intermodulation products (see Fig. 1) is considered a symptom of deterioration and a loss of quality of the device or material studied. For example, in the case of loudspeakers, a catalog of non-linearities associated with defects or deterioration of specific parts could be defined. A previous publication (Klippel 2006) addressed the relationship between non-linear distortion measurements and non-linearities, which are the physical causes for signal distortion in loudspeakers, headphones, micro-speakers and other transducers. Special mention deserve the application of exponential swept sine excitation signals, which allow to deconvolve simultaneously the linear impulse response of the system, and separate impulse responses for each harmonic distortion order (Farina 2000; Novak et al. 2010; Novak et al. 2015; Burrascano et al. 2019). A new simple and easy to implement method, termed as the Scaling Subtraction Method (SSM), has been proposed for enhancing the capabilities of detection of the non-linear elastic response of a system (Scalerandi et al. 2008; Antonaci et al. 2010; Antonaci et al. 2013).

Figure 1 shows graphically the concepts of harmonic distortion (HD) and intermodulation distortion (IMD) (Price and Goble 1993). HD takes place when a system is excited by a signal of frequency f_1 . In this case, higher order frequencies appear at the output ($f_2 = 2f_1$, $f_3 = 3f_1$, and so on), being this phenomenon termed as higher order harmonics generation (Fig. 1a).

IMD occurs at frequencies that are the sum and/or the difference of integer multiples of the fundamental frequencies. If a non-linear system is excited by two signals (f_1 and f_0), the non-linearity give rise to additional output components at $(f_1 + f_0)$ and $(f_1 - f_0)$ known as the first-order intermodulation products. At the same time, the second-order products will mix with the original signals

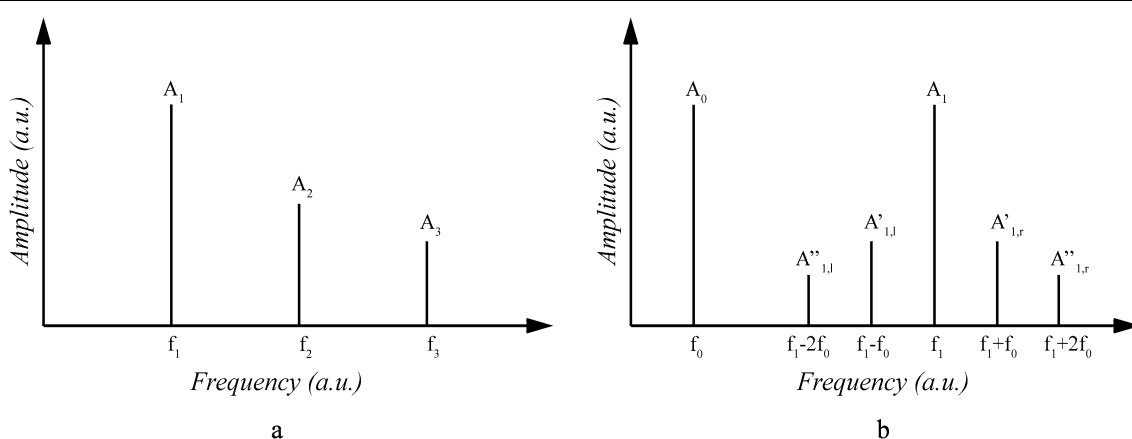


Fig. 1 Frequency spectrum: **a** harmonic distortion (HD); **b** intermodulation distortion (IMD).

giving components of frequencies ($f_1 + 2f_0$), ($f_1 - 2f_0$), and so on (see Fig. 1b).

Some reviews on the application of NLU techniques for non-destructive assessment of micro-damage in materials can be found in previous publications (Jhang, 2000, 2009). These techniques have been used to characterize the damage of granite samples subjected to compressive loadings (Chen et al. 2014) and to investigate thermal damage in sandstone (Chen et al. 2017). Several works have been devoted to the study of damage of concrete induced by loading (Antonaci et al. 2010; Kim et al. 2018). One problem associated with ultrasonic inspections of concrete structures is the high degree of signal attenuation, due to absorption and scattering (including backscattering) by the cement paste and aggregates. These phenomena lead to severe difficulties when there is only a single-side concrete surface available (pitch-catch inspection mode). The use of a combination of pulse-compression, low-frequency coded waveforms and piezo-composite transducers, has allowed to successfully overcoming these problems (Battaglini et al. 2014; Mohamed and Laureti 2015). For instance, the technique allowed detecting a steel rebar at a cover depth of 55 mm below the tested concrete surface in pitch-catch inspection mode (Laureti et al. 2018).

Only a few NLU studies of reinforcing steel corrosion in concrete can be found in the literature (Kwun et al. 1993; Woodward and Amin 2008; Korenska 2009; Antonaci et al. 2013).

Given the potential of the NLU techniques in terms of early damage detection and sensitivity to distributed micro-damage in materials, it was considered worth gaining more experience on the applicability of higher-harmonic and intermodulation product's generation to the study of micro-cracking induced by steel corrosion processes in cement-based materials. For this purpose, several prismatic reinforced cement mortar specimens were prepared and subjected to accelerated corrosion tests using an imposed electric field, while performing NLU measurements. The corrosion tests were conducted in conditions typical of experiments aimed at studying the evolution of the surface cracking due to steel corrosion (Andrade et al. 1993). The results presented in this work indicate that the appearance of visible surface micro-cracks seems to be preceded and accompanied by the observation of strong non-linear features in the received signal: harmonic distortion and intermodulation phenomena are clearly observed. However, it is hypothesized a possible influence of the filling of the cracks with liquid containing steel corrosion products on the evolution of the results of the

NLU measurements. This possible effect had not been pointed out before.

2 Materials and Methods

2.1 Sample Preparation

The experimental tests were performed on a set of three prismatic reinforced cement mortar specimens having the same dimensions and composition. These specimens were designated as specimens 9, 10 and 11. The choice of using cement mortar instead of concrete was due to the interest in using a more homogeneous and simple model material, by avoiding the presence of coarse aggregate, which could produce a higher heterogeneity of the composite material and possibly a higher wave attenuation and scattering (Battaglini 2014), as compared to the siliceous sand (maximum size 4 mm), used as the aggregate in the mortar mix.

First, the cement mortar was prepared mixing a standard siliceous sand aggregate and a sulphate resisting ordinary Portland cement, CEM I 52.5 R-SR 3, in accordance with the UNE-EN 197-1 standard (Asociación Española de Normalización y Certificación 2011). A kneading process was performed mixing the cement mortar with water containing dissolved sodium chloride (NaCl), being the water/cement mass ratio (*w/c*) 0.5. The admixed NaCl let obtain a content of 2% Cl⁻ relative to the cement weight in the hardened mortar (Climent et al. 2004), thus ensuring that the current efficiency of the electrically accelerated corrosion process be close to 100% (Nosseni and Harichandran 2012). In a following step, the fresh cement mortar mix was poured in 100 × 100 × 350 mm³ plastic molds before being mechanically compacted (manual compaction) and cured during 7 days in a humidity chamber at 20 °C and 95% relative humidity. Each of these molds allowed center-crossing a steel rebar of 12 mm in diameter along each sample, 10 mm beneath its upper surface. The steel bars were previously cleaned from native corrosion products following a recommended procedure (ASTM G1-03 2004) and weighted, covering the ends with vinyl electric tape to avoid the steel–mortar–air interface. This layout was chosen so as to favor the micro-cracking produced by the corrosion process to emerge on the upper surface of the samples and thus facilitate the monitoring of the micro-crack width growth over time using a microscope (Andrade et al. 1993; Alonso et al. 1998). More details of the experimental procedure can be found in a previous publication (Climent et al. 2019). The composition data of the cement mortar mix are given in Table 1. Figure 2 shows the layout and dimensions of the reinforced cement mortar specimens, and a photo of one of them before starting the corrosion test.

Table 1 Composition of mortar specimens.

Material	Amount (g)
Cement (CEM I 52,5 R SR(3))	450
Standard siliceous sand	1350
Deionized water	225 ($w/c = 0.5$)
NaCl	14.8 (2% Cl^- relative to cement weight)

2.2 Accelerated Corrosion Test

The accelerated corrosion tests were conducted using a potentiostat–galvanostat (Model 362, EG&G Instruments, Princeton NJ, USA). A constant anodic current density of $40 \mu\text{A}/\text{cm}^2$ was applied between the steel rebar (anode) and an external galvanized steel grid (cathode) placed in the bottom of the specimens. To keep an appropriate electrical conductivity throughout the cement mortar, the samples were partially submerged (5 mm height) in a recipient filled with tap water, and a polypropylene sponge was put between the mortar specimen and the steel grid (Climent et al. 2006). The duration of the accelerated corrosion tests was different for each one of the tested specimens, see Sect. 3.1. Given that the galvanostat provided a constant current density, it was possible to corrode three specimens simultaneously by connecting them in series. The tests were performed under nearly controlled climatic conditions, with a relative humidity of $84\% \pm 4\%$ and a temperature of $23 \pm 1^\circ\text{C}$, to minimize the influence of additional factors on the measurements, i.e., to avoid uncontrolled drying of the reinforced mortar specimens (Payan et al. 2010). Figure 3 shows an image of the accelerated corrosion test.

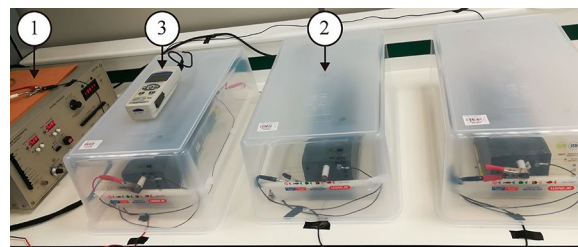


Fig. 3 Setup of the accelerated corrosion test. 1: potentiostat–galvanostat. 2: mortar specimen under test (the specimen is located on a tray with a plastic cover to keep a practically constant relative humidity environment, see text in Sect. 2.2). 3: relative humidity measurement device.

In this work, the physical damage of the cement mortar due to corrosion of the embedded steel bars has been followed by detecting the appearance of the first surface micro-crack and by monitoring the growth of the crack width over time. The monitoring process was possible because of the chosen setup and geometric conditions of the experiments, in which the cracks produced by steel corrosion appeared at the upper surface of the mortar specimen. A periodic inspection (daily measurements) of the mortar sample surfaces was carried out throughout the whole experiment using a microscope (magnification $40\times$, model 58-C0218, Controls, Milan, Italy). The limit of detection of the microscopic observations was approximately $10 \mu\text{m}$ (half value of the magnitude of the minimum division of the scale bar of the microscope: $20 \mu\text{m}$). For each measurement the whole upper surface of the mortar specimens was inspected in order to detect the first observable crack, or to record the maximum value of the crack width. Most of the times the maximum value of the crack width was recorded at the same place where the first crack was observed, only in on a few occasions

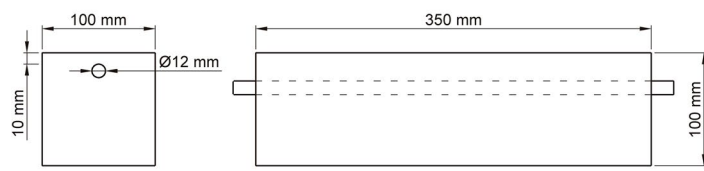
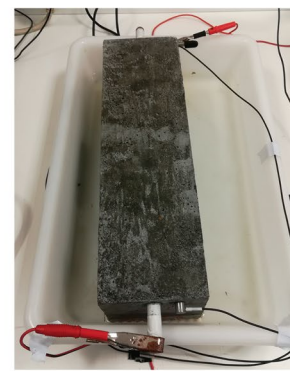
**a****b**

Fig. 2 **a** Dimensions of the reinforced cement mortar specimens. **b** Photo of one of the specimens before starting the corrosion test.

the maximum crack width was recorded at a different position. Microscopic photographs were also taken daily on selected positions at the upper surface of the samples. In this way it was possible to plot the maximum crack width growth as a function of time, see Sect. 3.1. According to observations of previous publications (Alonso et al. 1998), the crack width growth should be approximately linear during the propagation period of the process of mortar cracking due to steel rebar corrosion.

Another objective of this part of the research was to inspect the morphology of the steel–mortar interface and that of the open micro-cracks produced by the corrosion process. To this end the tests of the three reinforced mortar specimens were interrupted at different times, transversal cuts were performed on the tested specimens, and photographs were taken showing the aspect of the steel–mortar interface and that of the cracked mortar covering the bar.

2.3 Experimental Setup and Procedure of the Non-linear Ultrasonic Measurements

The experimental setup for the NLU measurements is shown in Fig. 4. They were conducted by means of a NI-USB 6361 multifunction I/O device with a sample frequency of 2 MS/s and an ACD resolution of 16-bits. For the HD experiments a 30 kHz sinusoidal signal with a length of 10,000 cycles was sent to a FS WMA-100 voltage amplifier and then to the emitter transducer. Amplitudes between 120 to 200 V in 10 V steps were used for the excitation signal. The received signal was

amplified using a signal conditioner 2693-A (Brüel & Kjaer, Naerum, Denmark) and then sent to the acquisition platform. For the IMD experiments, the emitter transducer was supplied with two tones at the same time ($f_1=30$ kHz, $f_0=2$ kHz).

IDK09 transducers (Dakel 2019) with isolated contact membrane (Al_2O_3 pure ceramic) and piezoelectric ceramic active element PbZrTiO_3 (PZT)—modified ceramic class 200—were used for both the emitter and receiver elements. This kind of PZT material is suitable for active (exciter) and passive (sensor) applications, and it is recommended for wide-band no-resonance uses due to their low mechanical quality factor ($Q_m < 100$). Both transducers were glued permanently (at the beginning of the NLU measurement series) to the reinforced cement mortar specimens using a quick setting Cyanoacrylate glue as the coupling agent. In this way it is thought that any possible defect or air void in the coupling interface has affected equally to all the NLU measurements. Taking into account that in this work the interpretation of the NLU data is always done on a comparative basis (no absolute value is considered), it is believed that the influence of the coupling between sample and transducers is negligible. Previous works (Antonaci et al. 2013) have also shown that that the effects due to small differences in coupling turned out to be negligible compared to the effects induced by corrosion of steel embedded in concrete. The NLU measurements were conducted on a “direct transmission” mode (Antonaci et al. 2013). Figure 5 shows a layout of the reinforced cement mortar

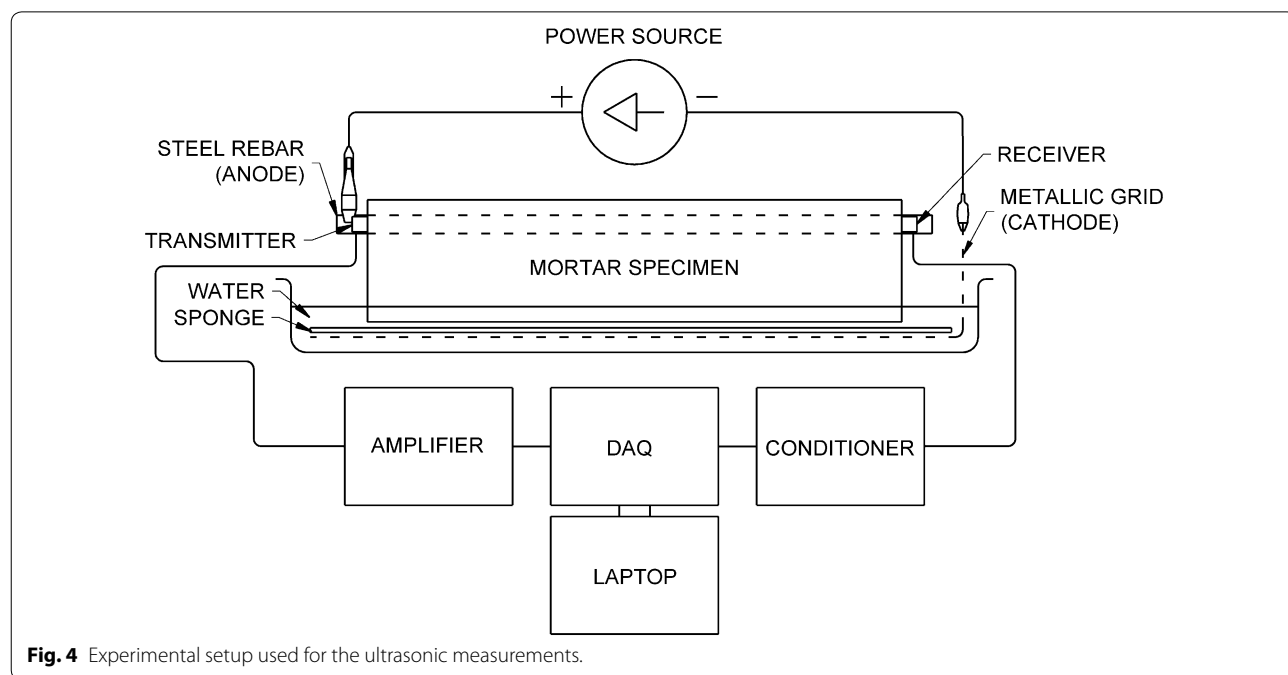


Fig. 4 Experimental setup used for the ultrasonic measurements.

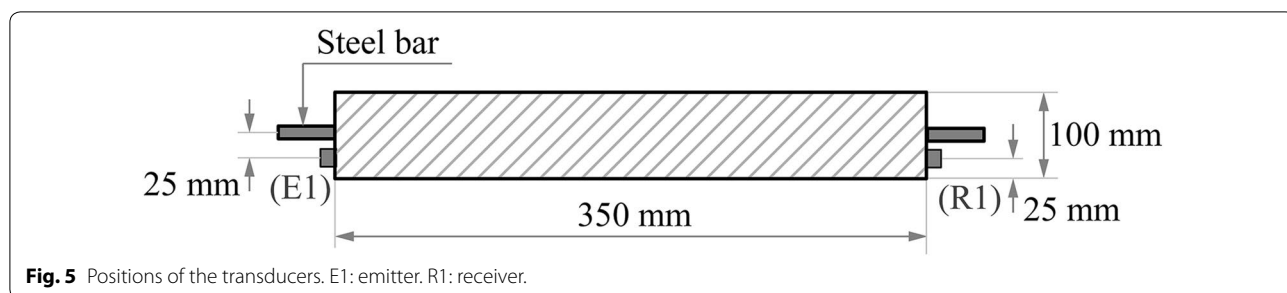


Fig. 5 Positions of the transducers. E1: emitter. R1: receiver.

specimen with the positions of the ultrasonic transducers and the steel bar under test.

The NLU measurements began always 1 day before the corresponding accelerated corrosion test. Two daily measurements (intervals of 12 h) were taken in the course of the experiments. In order to carry out the measurements, a custom-made application was implemented using the system-design development software LabVIEW® (see Fig. 6). The application allowed the emission and signal acquisition by automatically establishing different voltage steps according to the configuration indicated by the user.

A rectangular window was applied to the steady-state interval of the received signal. The frequency spectrum of the windowed signal was obtained using the Fourier transform method (FFT algorithm). Then, the amplitudes of the fundamental (corresponding to 30 kHz), second (60 kHz) and third harmonic (90 kHz) were determined. A similar process was carried out for the intermodulation products (first-order intermodulation products are expected at 28 and 32 kHz and second-order products near 34 and 26 kHz).

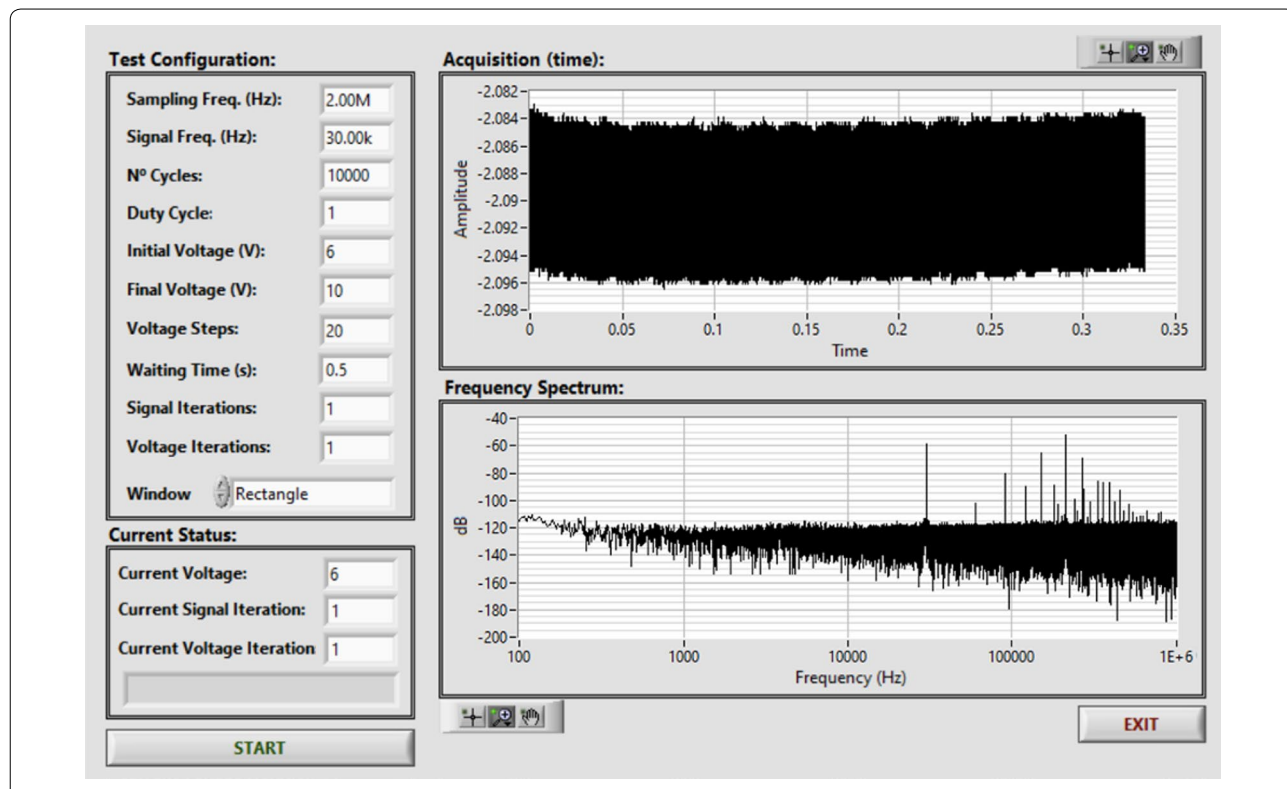


Fig. 6 Emission and signal acquisition application front panel.

2.4 Assessment of Material Damage Through Non-linear Elastic Wave Features

In the framework concerned the degradation of a material is linked to a non-linear mechanical behavior (Jhang 2000). As a result, when an ultrasonic wave propagates through the material and interacts with the microstructural defects, non-linear terms linked to these higher order waves are generated. As the micro-damage grows, non-linearity should increase.

Four different strategies have been used in this work to put in evidence the appearance of non-linear features due to the micro-damage of the specimens under study. First, the observation of the frequency spectrum of the received signal, which may allow direct observation of the higher harmonic generation or intermodulation distortion features; see Fig. 1. In second place the non-linearity parameters can be derived from the amplitudes of the fundamental and harmonic frequencies. Assuming that changes in the wave propagation velocity and the attenuation are small, and in experimental conditions like those used in this work (NLU measurements done with an input signal of fixed frequency, and the transducers located always at the same positions), the parameters of non-linearity can be approximated (Raichel 2006) as: $Bn = A_2/A_1^2$, and $Bpn = A_3/A_1^3$, being A_1 , A_2 and A_3 the amplitudes of the fundamental, second and third harmonic waves, respectively. In practice, the variation of these ratios relative to the initial undamaged conditions is used as an indicator of the microstructural damage (Shah and Ribakov 2009b).

As for specific parameters that have been used to quantify the damage by incorporating intermodulation products, the intensity modulation ratio, R , defined as:

$$R = \frac{A'_{1,l} + A'_{1,r} + A''_{1,l} + A''_{1,r}}{A_1}, \quad (1)$$

where $A'_{1,b}$, $A'_{1,r}$, $A''_{1,l}$ and $A''_{1,r}$ are the amplitudes of the subsequent left and right sidebands, respectively, and A_1 is the amplitude of the high-frequency acoustic wave; see Fig. 1. The intensity of the modulation ratio can be correlated with damage size. In many studies, the parameter R has been used as the damage index (Van den Abeele et al. 2000; Friswell and Penny 2002; Muller et al. 2005; Aymerich and Staszewski 2010).

In this work it is proposed the use of a new parameter for putting in evidence the micro-damage through the intermodulation non-linear features. The new index, termed as $DIFA$ (difference of amplitudes), Eq. (2), is based on the difference between the amplitude of the fundamental frequency and the sum of the amplitudes of all the first-order and second-order intermodulation products; see Fig. 1:

$$DIFA = A_1 - (A'_{1,l} + A'_{1,r} + A''_{1,l} + A''_{1,r}). \quad (2)$$

The parameter $DIFA$, as R , is thought to be sensitive to both the non-linear effects on the fundamental frequency (decrease of amplitude) and on the intermodulation products (increase of amplitudes). However, it also can be considered to represent somehow the redistribution of elastic energy among the various generated frequencies of the signal (Scaleraudi et al. 2008). If $DIFA$ shows a high value, close to the value corresponding to a reference (non-damaged) state, it would be indicating a low transference of energy to the intermodulation products. Conversely, a very low value of $DIFA$, as compared to the reference value, might be representative of a high degree of redistribution of elastic energy due to the appearance of critical micro-defects able to enhance the non-linear features of the elastic response.

3 Results and Discussion

3.1 Observations of the Evolution of the Damage due to Steel Corrosion

In the experimental conditions of these tests, the penetration of the steel corrosion process can be considered as linear with time, being the corrosion rate equal to the anodic current density passing through the electric circuit, i.e., the current efficiency is close to 100% (Nosseni and Harichandran 2012; Climent et al. 2019). Hence, the loss of effective radius of the steel bar, x , can be calculated as (Molina et al. 1993):

$$x = 0.0319 \cdot I_{corr} \cdot t, \quad (3)$$

where x is expressed in μm , I_{corr} is the constant anodic current density expressed in $\mu\text{A}/\text{cm}^2$ (in this work $40 \mu\text{A}/\text{cm}^2$), and t is the time elapsed since the beginning of the accelerated corrosion test, in days. The value 0.0319 contains all relevant physical constants and unit change factors that are needed for the calculation.

It must be recalled here that the accelerated corrosion test (current passing on) started always 1 day after beginning the series of NLU measurements, in order to

Table 2 Data corresponding to the accelerated corrosion tests conducted on the three reinforced cement mortar specimens.

Sample	First crack (days)	x_0 (μm)	End of the test (days)
9	10 (9)	11.5	31 (30)
10	9 (8)	10.2	15 (14)
11	8 (7)	8.9	8 (7)

Data in parentheses are the days elapsed from the onset of current passing.

have a reference value regarding these variables. Table 2 contains the most relevant data of the experiments conducted on the three reinforced cement mortar specimens. The second column of the table contains the days elapsed when the first micro-crack was observed on each one of the specimens, see Sect. 2.2. Data in parentheses correspond to the days elapsed since the onset of current passing. The third column shows the values of the corrosion penetration necessary to produce the first visible crack (x_0), calculated using Eq. (3) and the times indicated in parentheses at the second column of the table. Finally, the fourth column contains the time at which each test was finished: at these times the NLU measurements were discontinued and the specimens were cut for observation of the steel–mortar interface and of the cracked mortar covering the rebar.

The first micro-crack in sample 11 was detected on the eighth day (7 days of current passing). Then, the specimen was disconnected from the power supply. A day later, a visible crack appeared in sample 10, and 2 days later it appeared in sample 9 (see Table 2). The test of sample 10 was stopped at the 15th day, and after disconnecting the current the specimen was cut in order to inspect the fissure and the corrosion products path; see Fig. 7. On that 15th day the maximum crack width on the upper surface of sample 10 reached the value of 70 μm . Finally, the test of sample 9 was concluded after 31 days of testing, when the surface of the specimen showed a crack with a maximum value of 320 μm width. Figure 7 shows clearly the accumulation of steel corrosion products at the steel–mortar interface, especially on top of the

bar, and the partial filling of the open crack produced by the corrosion process.

Figure 8 shows a series of images corresponding to the evolution of the fissure appeared on top of the mortar specimen number 9. The figure also includes the measured values of the crack width.

Another remarkable observation regarding the accelerated corrosion tests is that after the appearance of the open crack on top of the mortar specimens, a reddish viscous liquid, containing also solid steel corrosion products, leached out through the cracks; see Fig. 9. The pH of this liquid was 3, because of the hydrolysis reaction caused by the iron ions in solution (Andrade et al. 1993; Climent et al. 2019). This implies that a net mass transport process is taking place through the mortar specimens. It is known that transport phenomena through porous media, for instance ion diffusion, are greatly enhanced in case of exposure to a humid environment (Climent et al. 1998). Furthermore, a convective transport process can take place due to liquid wick action through concrete (Aldred et al. 2004), in the case of experimental conditions like those in this work: contact with liquid water at the lower part of the mortar specimen and exposure of the rest of surfaces to an atmosphere of relative humidity lower than 100%. The net transport of water from the bottom of the specimen to the upper surfaces drags the steel corrosion products first filling the cracks and finally making them appear at the openings of the cracks on the top surface; see Figs. 7, 9. However, it was observed that the leaching phenomenon was of different intensity for the various specimens under test. Figure 9 clearly shows that the leaching appeared earlier and with a much higher intensity for specimen number 9 than for specimen number 10. See the upper surfaces of both specimens at the 12th and 14th days of testing, and the much higher accumulation of reddish iron corrosion products in the plastic tray supporting specimen 9. The most likely explanation for this different intensity of the leaching of corrosion products is a possible difference in the compaction of the reinforced cement mortar specimens. It must be recalled that the compaction was done manually, see Sect. 2.1. It is possible that if the steel–mortar interface was less compact and more imperfect in some case (specimen 9), the dragging of corrosion species formed at the steel surface may have been more efficient, thus leading to a quicker filling of the cracks and to a more intense leaching out of corrosion products.

Figure 10 depicts the evolution of the crack width for the mortar specimens, as a function of time. The cracking of concrete due to stresses caused by corrosion of embedded steel has been classically described as consisting of a short period during which no crack is visible; the generation step, followed by an approximately linear



Fig. 7 Photo taken after cutting specimen number 10, at the end of its corrosion test. Steel corrosion products have concentrated on top of the steel rebar and are filling the open crack produced by corrosion.



Fig. 8 Images corresponding to the evolution of the maximum size of the crack on top of the mortar specimen number 9.

increase of the crack width; the propagation period of the cracking process (Alonso et al. 1998; Andrade et al. 1993; Molina et al. 1993; Pedrosa and Andrade 2017). Nevertheless, some critical events can be considered in this process. The first appearance of an open crack at one of the exterior faces of the concrete specimen means that the incipient micro-cracks that may have been developing within the cementitious matrix, probably starting at the steel–cement paste interface, have coalesced to form a continuous crack which finally opens to the concrete surface (Antonaci et al. 2013). This implies an event where the composite material has increased considerably its heterogeneity (creation of new void space),

thus changing considerably its non-linear elastic properties. In this sense it must be considered that for the three specimens the non-linear features should have increased considerably between the days 8th to 10th; see Fig. 10 and Table 2. Furthermore, even though the propagation is described approximately as a period of linear increase of the crack width, some changes of slope are clearly visible in Fig. 10. See for instance the sudden increase of maximum crack width between the 21st and 22nd days for specimen 9. These sudden changes are also probably due to creation of new void space, it may be the expansion of an existing crack or creation of a new open crack. Hence, it should also be expected to find observation

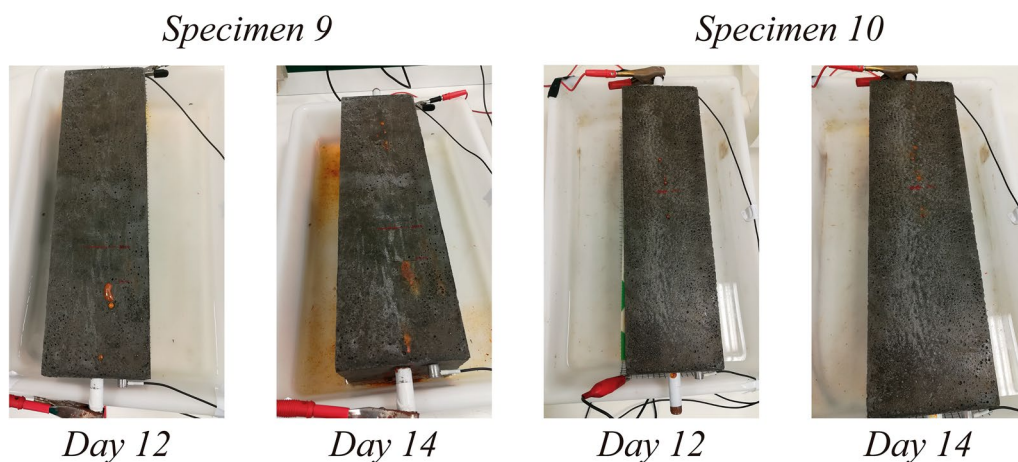


Fig. 9 Photos of specimens number 9 and 10 showing a difference of the intensity of the leaching out of steel corrosion products through the open cracks.

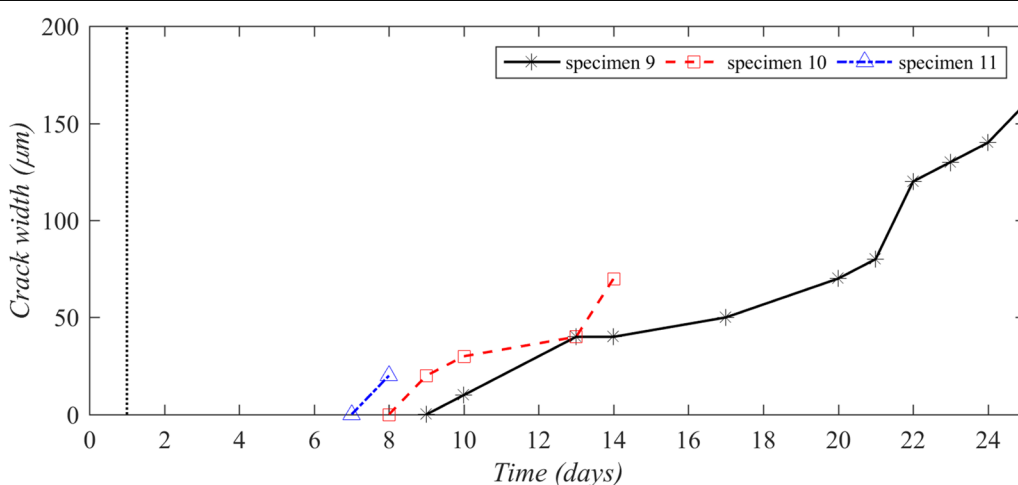


Fig. 10 Crack width evolution measured for the three specimens.

of increased non-linear features associated with these changes of slope in Fig. 10.

Regarding the corrosion penetration necessary to produce the first visible crack (x_0), it can be calculated using a previously proposed empirical equation (Alonso et al. 1998):

$$x_0(\mu\text{m}) = 7,53 + 9,32 \cdot \frac{c}{\varnothing}, \quad (4)$$

where c is the concrete cover depth over the rebar and \varnothing is the diameter of the rebar. Using Eq. (4) with the corresponding values of the geometric parameters of this work, a value of 15 μm is obtained for x_0 . This calculated value is slightly higher than the experimental values shown in the third column of Table 2, whose mean value

is $10.2 \mu\text{m} \pm 1.3 \mu\text{m}$. However, it must be considered that Eq. (4) was derived by linear fitting of a data set of experimental results obtained in accelerated corrosion tests with a current density of $100 \mu\text{A}/\text{cm}^2$ (Alonso et al. 1998), while a current density of $40 \mu\text{A}/\text{cm}^2$ has been applied in this work. The authors of the above-mentioned study (Alonso et al. 1998) confirmed the influence of the current density applied. The lower the current density was, the faster the first crack appeared (less attack penetration needed) and the faster it developed. This may be interpreted mechanically by considering that a slower "load" application induces higher deformations (Alonso et al. 1998; Pedrosa and Andrade 2017). As a consequence, the results presented in this work can be considered as being

in fairly good agreement with the observations of previous authors.

3.2 Ultrasonic Tests

This section presents the results of the NLU measurements performed on the three reinforced cement mortar specimens under test. These measurements started always 1 day before the beginning of the corresponding accelerated corrosion test, i.e., 1 day before switching on the current; see Sect. 2.3. Some of the figures in this section show a vertical line indicating the onset of the corrosion test ($t=1$ day).

Figure 11 shows the results derived from the analysis of the frequency spectra of the received signals corresponding to specimen 10. The results correspond to the day 0 (before the onset of the corrosion test), and the days 3, 7 and 10. The relative amplitude of the components of each frequency spectrum was always calculated taking the reference amplitude (A_{ref}) as equal to 1 V. Hence, the relative value of any amplitude (A) depicted in Fig. 11 has been calculated according to the following expression:

$$\text{Relative amplitude}(dB) = 10 \cdot \log \frac{A}{A_{ref}}. \quad (5)$$

It is apparent from Fig. 11 that the amplitudes of the second and third harmonics (A_2 and A_3) are always far lower (more than 30 dB lower) than the fundamental amplitude (A_1). At this point it should be recalled that

the first visible crack due to steel corrosion was detected on the surface of specimen 10 at the ninth day (Fig. 10 and Table 2). Regarding the evolutions of the relative amplitudes in Fig. 11, it is appreciable that on the third day small differences were found in comparison with the day 0 (before the onset of the corrosion test): the fundamental amplitude decreased slightly, and the harmonics' amplitudes also showed small differences with their amplitudes at the day 0. However, on the 7th day, 2 days before the visible appearance of the micro-crack at the surface of the mortar specimen, a strong decrease of the fundamental amplitude (about 20 dB) was observed together with comparatively lower (about 10 dB) reductions of the amplitudes of the harmonics. These differences can be clearly ascribed to harmonic distortion phenomena. Three days later (10th day) the relative values of the amplitudes returned to values close to those found on the 3rd day. The observations on the 7th day are compatible with a strong increase of the non-linear elastic features: previous publications have clearly shown that the effects of a non-linear elastic feature on the amplitude of the fundamental frequency component of the signal are much stronger than those on the second- and third-order harmonic components (Scaleraudi et al. 2008). It is reasonable to interpret that on the 7th day, few days before the observation of the first visible surface fissure, the micro-cracks were actively developing at the cement mortar cover region over the corroding steel rebar. This observation points out to the possibility that the NLU measurements may provide an early warning of the cracking due to steel corrosion.

Figure 12 shows the variations of the relative values of the parameters B_n and B_{pn} during the tests of the three reinforced mortar specimens. Any value in the figure is normalized to its corresponding value at ($t=0$). It must be recalled that the values of these B_n and B_{pn} parameters are proportional to those of the rigorously defined non-linearity parameters; see Sect. 2.4. Previously it was proposed a tenfold increase relative to the initial values of these parameters, as the arbitrary threshold for considering a critical increase of the non-linear elastic features, which in turn would be indicative of the presence of significant defects or damage in the material medium (Climent et al. 2019). This threshold is indicated as dotted horizontal lines in the plots of Fig. 12. Regarding the results corresponding to specimen 11 (blue triangle points in Fig. 12), the relative parameters exceeded clearly the arbitrary threshold for the measurements taken during the interval between the 6th and the 8th day when a visible crack was first observed at the upper surface of specimen 11; see Table 2 and Fig. 10. As for the results of specimen 10 (red square points in Fig. 12), the relative

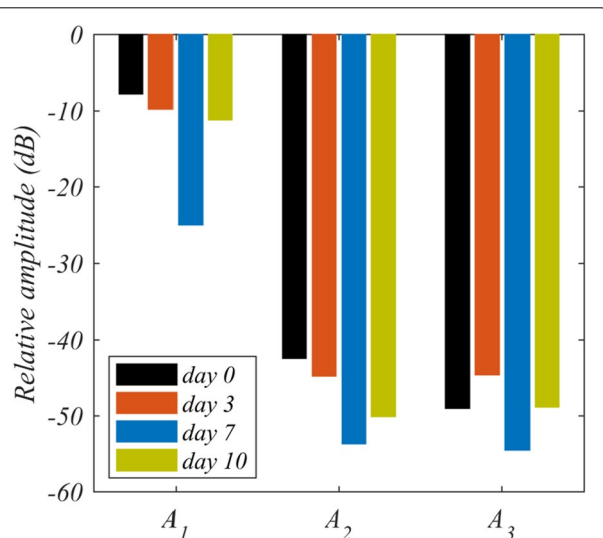


Fig. 11 Relative amplitude evolution of the main components of the frequency spectrum of the received signal for specimen 10 (transducer emitter excited with 180 V). A_1 : relative amplitude of the fundamental frequency ($f_1=30$ kHz). A_2 and A_3 : relative amplitudes of the second and third harmonics, respectively, ($f_2=60$ kHz and $f_3=90$ kHz).

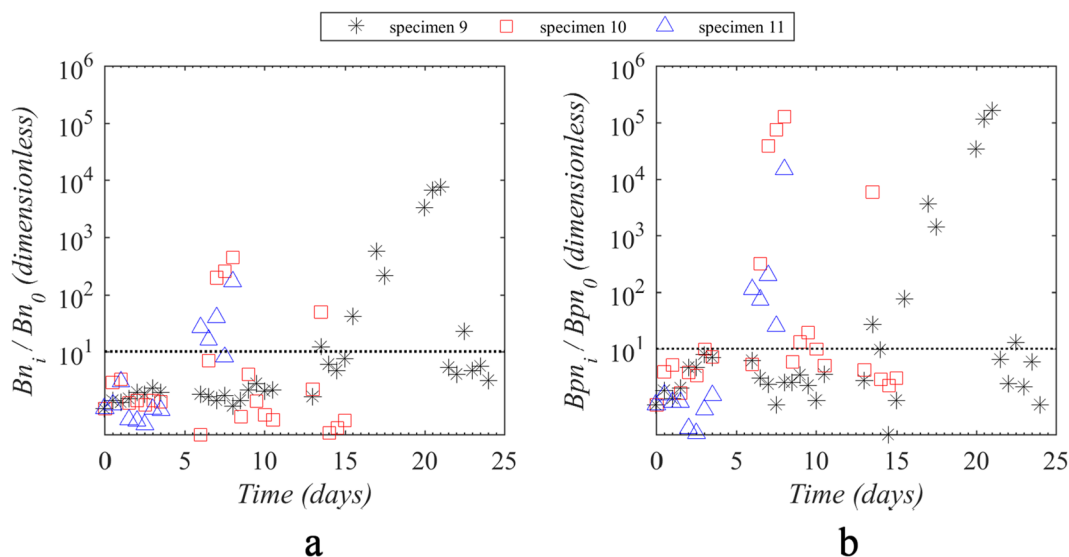


Fig. 12 Evolution of the parameters Bn and Bpn , normalized to their initial values ($t=0$), during the tests of the three reinforced cement mortar specimens (transducer emitter excited with 180 V). The dotted horizontal line represents the arbitrary threshold considered as indicative of a critical increase of the non-linear elastic features, see text for details.

parameters were clearly higher than the tenfold threshold in the period between the 7th and the 10th days of measurements. Looking at Fig. 10, it is appreciable that this period correspond to the few days around the moment of first observation of the surface crack on top of specimen 10 (9th day). However, after the 10th day the relative values of Bn and Bpn returned to the region below the tenfold threshold, except for a single measurement obtained on the 13th day. Finally, the results corresponding to specimen 9 (black star points in Fig. 12) show a different behavior: the relative values of Bn and Bpn did not exceed the threshold during the days around the first observation of a crack on top of specimen 9 (10th day). Instead, the parameters reached values much higher than the tenfold threshold during the period between the 15th and 21st days. It should be noted from Fig. 10 that these days preceded a clear change of slope in the evolution of the surface crack width growth, observed between the 21st and 22nd days for specimen 9. Hence, it is highly probable that all the observed strong increases of the values of the relative values of Bn and Bpn exceeding the arbitrary threshold, may be correlated with damage of the material related to the corrosion process: creation of a new open crack or creation of new void space by considerable enlargement of the width of an existing crack (Shah and Ribakov 2009b; Climent et al. 2019). Another observation appreciable from Fig. 12 is that the parameter Bpn (related to the third harmonic) seems to be comparatively more sensible than the parameter Bn

(related to the second harmonic) for detecting the non-linear features associated with damage due to embedded steel corrosion in cement mortar.

As for the experiments of intermodulation, Fig. 13, Fig. 14 depict the evolutions with time of the values of parameters R and $DIFA$, respectively. The parameters are defined in Sect. 2.4, Eq. (1) and Eq. (2), respectively. Regarding the intensity modulation ratio, Fig. 13 shows rather clear progressive increases of the values of R during the critical time periods related with the cracking due to corrosion: for specimens 9 and 10, R started to increase just after the onset of the accelerated corrosion test, from days 1st to 9th, i.e., during the period when the micro-cracks are thought to be developing before coalescing into an open crack, which was visible on the upper surface at the 10th and 9th days for specimens 9 and 10, respectively (Table 2 and Fig. 10). The results of specimen 11 were less clear in this sense. Furthermore, another maintained progressive increase of R is observed for specimen 9 during the days 17th to 21st in parallel with the observation of high values of the relative Bpn parameter of specimen 9 in Fig. 12. It should be noted also that after these periods of progressive increase of R , its values decrease to lower values, making Fig. 13 to look like a saw-teeth graph. It seems that the IMD phenomena might be present long before the first observation of cracking, although some uncertainty remains regarding some results showing small increases of R (specimen 11).

Figure 14 shows the variations of the parameter $DIFA$ as a function of time for the tests of the reinforced mortar

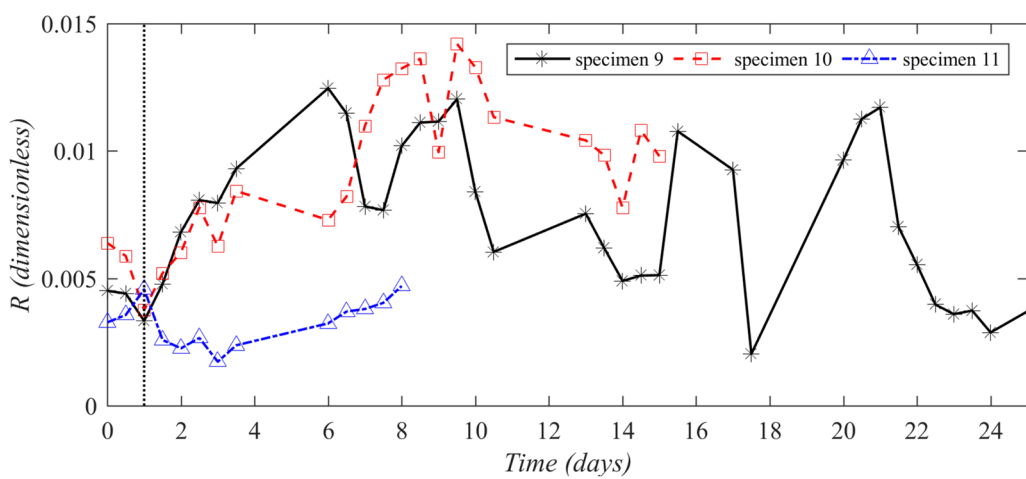


Fig. 13 Evolutions of the values of parameter R with time. The emitter transducer was supplied with two tones at the same time ($f_1 = 30$ kHz, $f_0 = 2$ kHz), and excited with 180 V. The vertical line ($t = 1$ day) indicates the onset of the accelerated corrosion test.

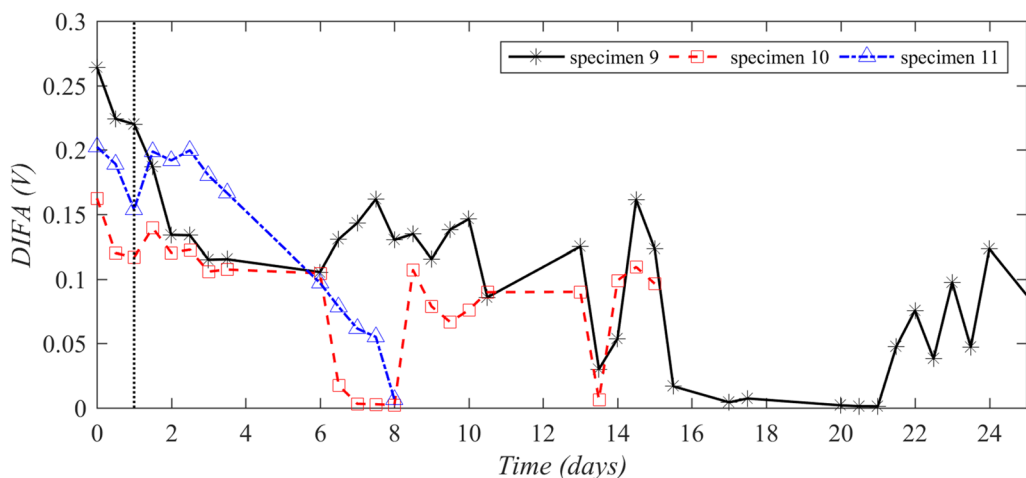


Fig. 14 Evolutions of values of the parameter DIFA with time. The vertical line ($t = 1$ day) indicates the onset of the accelerated corrosion test.

specimens. It is appreciable that after the onset of current passing slight decreases of the parameter were observed for the three specimens. However, the most relevant variations were recorded between the days 6th and 8th for the specimens 10 and 11, and between the days 15th to 21st for specimen 9. During these latter periods the parameter DIFA dropped rather abruptly to very low values, close to 0, thus indicating a strong non-linear elastic response. This feature is not so evident when analyzing the evolutions of the dimensionless relative parameter R with time (Fig. 13). An excellent correlation may be noted between the periods of very low values of DIFA (Fig. 14), and those of high values of the relative parameters Bn and Bpn exceeding the arbitrarily chosen threshold (Fig. 12).

Again, it is noticeable in Fig. 14 that after the periods of very low values, the parameter DIFA returns to intermediate values (about 0.1 V in these experiments) typical of the situation previous to the critical events of the cracking process.

Two issues remain unsolved in the preceding paragraphs. The first is the different behavior observed for specimen 9 in Figs. 12, 14, during the days 6th to 10th: the values of the relative parameters Bn and Bpn corresponding to this specimen did not exceed the tenfold threshold, and its values of the parameter DIFA did not drop to values close to 0. The second question is related with the ubiquitous observation that after the critical events of the cracking process, put in evidence by strong

non-linear features in the received ultrasonic signals (considerable decrease of the fundamental amplitude in Fig. 11, large increases of the relative parameters Bn and Bpn in Fig. 12, progressive increases of R in Fig. 13, and abrupt drops of $DIFA$ to values close to 0 in Fig. 14), all the parameters returned to values typical to the pre-critical situation. A possible explanation may be hypothetically formulated taking into account previous knowledge and the observations and discussion of the precedent Sect. 3.1. It is generally accepted, in studies of concrete cracking due to steel reinforcement corrosion, that when the corrosion process has started there are three propagation stages: a first stage in which the corrosion products penetrate the porous network around the steel rebar, filling the steel/concrete interface; a second stage characterized by stress initiation since the corrosion accommodation region is completely filled with rust products that start to exert stress; and a third stage identified by the formation of cracks when stress reaches the tensile strength of the concrete and rust fills the cracks as they are created, (Bazán et al. 2018). The experimental conditions of the tests in this work induce a continuous net liquid transport from the bottom of the cement mortar specimen (in contact with liquid water) to the upper surfaces, due to wick action (Aldred et al. 2004), see Sect. 3.1. This convective transport may drag the solid corrosion products formed at the surface of the steel bar, and may give rise to a more efficient filling of the new void space created by cracking with liquid containing corrosion products of steel. This might explain the returning of all the values of the parameters depicted in Figs. 11, 12, 13, 14 to values typical to the pre-crack situation, after having reached values indicative of strong non-linear elastic features. It is also possible that this circumstance might be especially important in cases where the steel–cement paste interface is somehow less compact, due for instance to a defective compaction; see Fig. 9 and the related discussion in Sect. 3.1 regarding the differences observed in relation to the leaching out of liquid containing rust products through the open cracks. This would be a plausible explanation for the different behavior shown by specimen 9 in Fig. 12, Fig. 14. It is known that when the rust products penetrate efficiently the porous network of the concrete, the pressure exerted by the expansion of the oxides is partially mitigated (Bazán et al. 2018). A careful observation of Fig. 10 allows appreciating that the first observed crack on top of specimen 9 appeared slightly later (10th day) than those appreciated on specimens 10 and 11 (9th and 8th days, respectively). Also, the first visible crack on specimen 9 had a width half of the value recorded for specimens 10 and 11. These observations seem to be indicative that the formation of the first visible crack on top of specimen 9 may have developed in a

different way than those corresponding to specimens 10 and 11. A more efficient filling of the crack would explain the delay of the observation of non-linear features associated with the cracking of specimen 9: these features were not observed at the time of formation of the first visible crack (10th day), but they were clearly appreciable during the period between the 15th and 21st days when the micro-cracks may have been developing and coalescing to give rise to a considerable enlargement of the maximum width of the surface crack; see Fig. 10 between the 21st and 22nd days. The effect of filling the new formed cracks with liquid containing rust products, and its possible impact on the results of the NLU measurements, may be of diverse magnitude when a different experimental approach is adopted for the accelerated corrosion test (Antonaci et al. 2013).

It is widely accepted in ultrasonic researches that there are many sources of non-linearity. Some doubts might be raised regarding the modification of the microstructure of the mortar specimens due to the progressive cement hydration and mechanical strength gain process: in this work the reinforced mortar specimens were tested after a period of curing of only 7 days (Sect. 2.1). However, it must be noted that the mortar was prepared with a cement of high speed of mechanical strength gain, CEM I 52.5 R-SR 3 (Asociación Española de Normalización y Certificación 2011). A standardized cement mortar using this type of cement reaches a minimum initial compressive strength of 30.0 MPa at 2 days, and a minimum nominal compressive strength of 52.5 MPa at 28 days. If we consider also the known accelerating effect of admixed chloride salts in relation to the mechanical strength gain of cement-based materials, it is reasonable to admit that the cement mortar has reached a considerable degree of development of cement hydration and mechanical strength during the 7 days curing, so as not to expect drastic changes in the microstructure that could give rise to relevant non-linear effects. Taking into account the good temporal correlation found between the critical events of mortar cracking recorded in Fig. 10 and Table 2, and the observations of relevant non-linear elastic features in the received ultrasonic signals (Figs. 11, 12, 13, 14), it is highly probable that these non-linear effects are mainly due to the damage produced by corrosion of the steel bars under the form of micro-cracks which eventually coalesce to create an open crack visible at the upper mortar surface.

The non-elastic features can be efficiently detected both through HD (Bn and Bpn parameters) or IMD (R and $DIFA$ parameters) experiments. The presented results suggest that the new parameter $DIFA$ proposed in this work is as efficient as the relative parameters Bn and Bpn for detecting the strong non-linear features associated

with the critical events of the cracking of cement mortar damage due to embedded steel corrosion. During these critical events it is likely that new micro-cracks are being formed, or other pre-existing cracks are actively developing before coalescing into an open surface crack or giving rise to a considerable and sudden enlargement of the maximum width of the surface crack. Hence, it is reasonable to admit that in these circumstances the ultrasonic waves travel through a highly defective medium, leading to a relevant transference of energy from the fundamental frequency component of the waveform to higher order harmonics or to the intermodulation products (Scaleraudi et al. 2008). These energy transferences manifest as highly increased values of the Bn and Bpn parameters or very low values of the $DIFA$ parameter. The evolution of values found for the intensity modulation ratio (R), seems to indicate that the non-linear features may be appearing some time before the observation of an open crack, thus giving support to the idea that NLU techniques might be used as tools for the early warning of incipient damage due to steel reinforcement corrosion in concrete, before the appearance of visible symptoms of damage (cracking or delamination).

More research is necessary to confirm the findings and interpretations of this work, and to advance on the proposal of practical procedures for applying the NLU techniques to the detection of cracks due to steel corrosion in reinforced concrete, both for research purposes and for routine engineering surveys of damaged structures.

4 Conclusions

The results obtained in this work provide further confirmation that it is possible to use NLU techniques for the detection of cracking due to the corrosion of steel reinforcements in cement mortar or concrete. The appearance of visible surface micro-cracks seems to be preceded and accompanied by the observation of strong non-linear features in the received signal: harmonic distortion and intermodulation phenomena are clearly observed. A new parameter ($DIFA$), based on the difference between the amplitude of the fundamental frequency and the sum of the amplitudes of all the first-order and second-order intermodulation products, has been proposed in this work. The results suggest that the parameter $DIFA$ is as efficient as the relative non-linearity parameters, classically used in harmonic distortion NLU studies, for detecting the strong non-linear features associated with the critical events of the cracking of cement mortar damage due to embedded steel corrosion.

A recurrent observation in this work is that after the critical events of the cracking process, all the parameters used for putting in evidence the non-linear elastic features returned to values typical to the pre-critical

situation. A hypothetical explanation to this fact has been developed in this work considering the possible effect of the filling of the void space by liquid containing steel corrosion products after the formation of new cracks or the enlargement of its width. This filling process might be particularly enhanced by net convective transport of liquid (wick action) in the experimental conditions of this work. More research is necessary to confirm the findings and interpretations of this work, and to advance on the proposal of practical procedures for applying the NLU techniques to the detection of cracks due to steel corrosion in reinforced concrete, both for research purposes and for routine engineering surveys of damaged structures.

Acknowledgements

We would like to thank Carmen Andrade for advice on the details of the corrosion testing. We thank also Lafarge-Holcim Spain for providing the cement samples for preparing the reinforced mortar specimens. M.M. acknowledges a pre-doctoral fellowship from the Spanish Ministerio de Educación, Cultura y Deporte (FPU16/04078).

Author's information

Authors' current positions: M.A.C. (Full Professor at the Civil Engineering Department); M.M. (PhD Student); P.P. (Researcher at DFISTS) and J.R. (Full Professor at DFISTS).

Authors' contributions

All authors contributed to the paper equally. This article will constitute part of the PhD thesis of M.M. All authors read and approved the final manuscript.

Funding

This research was funded by the Spanish Agencia Estatal de Investigación (Grant code BIA2016-80982-R) and by the European Regional Development Fund (Grant code BIA2016-80982-R).

Availability of data and materials

The experimental data used to support the observations of this study are included in the article.

Competing interests

The authors declare that they have no competing interests.

Author details

¹ Civil Engineering Department, University of Alicante, Sant Vicent del Raspeig, 03690 Alicante, Spain. ² DFISTS, University of Alicante, Sant Vicent del Raspeig, 03690 Alicante, Spain.

Received: 16 January 2020 Accepted: 5 August 2020

Published online: 06 October 2020

References

- Aldred, J. M., Rangan, B. V., & Buenfeld, N. R. (2004). Effect of initial moisture content on wick action through concrete. *Cement and Concrete Research*, 34(6), 907–912.
- Alonso, C., Andrade, C., Rodriguez, J., & Diez, J. M. (1998). Factors controlling cracking of concrete affected by reinforcement corrosion. *Materials and Structures*, 31(7), 435–441.
- American Concrete Institute, 1996, *Corrosion of metals in concrete: ACI Committee 222R-96*, Farmington Hills, 29 p.p.
- American Society for Testing and Materials, 1991, *Standard test method for half-cell potentials of uncoated reinforced steel in concrete: ASTM C876-91*, West Conshohocken.

- American Society for Testing and Materials, 2004. *Standard practice for preparing, cleaning, and evaluating corrosion test specimens: ASTM G1-03*, ASTM Special Technical Publication, West Conshohocken, 9 p.p.
- American Society for Testing and Materials, 2016. *Standard Test Method for Pulse Velocity Through Concrete: ASTM C597-16*, West Conshohocken.
- Andrade, C., Alonso C., Fullea J., Polimón J. & Rodriguez J. (Eds.), 2000, *Proceedings of the International Workshop on Measurement and Interpretation of the On-site Corrosion Rate (MESINA)*, Madrid, Spain, 22–23 February 1999: RILEM Publications, Cachan.
- Andrade, C., Alonso, C., & Molina, F. J. (1993). Cover cracking as a function of rebar corrosion. 1. *Experimental Test: Materials and Structures*, 26, 453–464.
- Andrade, C., & González, J. A. (1978). Quantitative measurements of corrosion rate of reinforcing steels embedded in concrete using polarization resistance measurements. *Werkstoffe und Korrosion*, 29, 515–519.
- Antonaci, P., Bocca, P., & Masera, D. (2012). Fatigue crack propagation monitoring by Acoustic Emission signal analysis. *Materials Structure and Micromechanics of Fracture*, 465, 370–373.
- Antonaci, P., Bruno, C. L., Gliozi, A. S., & Scalcerandi, M. (2010). Monitoring evolution of compressive damage in concrete with linear and nonlinear ultrasonic methods. *Cement and Concrete Research*, 40(7), 1106–1113.
- Antonaci, P., Bruno, C. L. E., Scalcerandi, M., & Tondolo, F. (2013). Effects of corrosion on linear and nonlinear elastic properties of reinforced concrete. *Cement and Concrete Research*, 51, 96–103.
- Asociación Española de Normalización y Certificación, 2011, Cemento. Parte 1: Composición, Especificaciones y Criterios de Conformidad de los Cementos Comunes (Cement. Part 1: Composition, Specifications and Conformity Criteria for Common Cements): UNE-EN 197-1; Equivalent to the European Standard EN 197-1, AENOR, Madrid, Spain, 38 p.p. (In Spanish)
- Aymerich, F., & Staszewski, W. J. (2010). Experimental study of impact-damage detection in composite laminates using a cross-modulation vibro-acoustic technique. *Structural Health Monitoring—an International Journal*, 9, 541–553.
- Battaglini, L., Laureti S., Ricci M., Burrascano P., Davis L. A. J. & Hutchins D. A., 2014, The use of pulse compression and frequency modulated continuous wave to improve ultrasonic non destructive evaluation of highly-scattering materials. In: *2014 IEEE International Ultrasonics Symposium*, p. 1940–1943, IEEE.
- Bazán, A. M., Gálvez, J. C., Reyes, E., & Galé-Lamuela, D. (2018). Study of the rust penetration and circumferential stresses in reinforced concrete at early stages of an accelerated corrosion test by means of combined SEM. *EDS and strain gauges: Construction and Building Materials*, 184, 655–667.
- Bertolini, L., Elsener, B., Pedeviari, P., Redaelli, E., & Polder, R. B. (2013). *Corrosion of steel in concrete: prevention, diagnosis, repair*. Hoboken: Wiley.
- Blitz, J., & Simpson, G. (1995). *Ultrasonic methods of non-destructive testing* (Vol. 2). Berlin: Springer Science & Business Media.
- Burrascano, P., Laureti, S., Ricci, M., Terenzi, A., Cecchi, S., Spinsante, S., et al. (2019). A swept-sine pulse compression procedure for an effective measurement of intermodulation distortion. *IEEE Transactions on Instrumentation and Measurement*, 69(4), 1708–1719. <https://doi.org/10.1109/TIM.2019.2912591>.
- Chen, J., Xu, Z., Yu, Y., & Yao, Y. P. (2014). Experimental characterization of granite damage using nonlinear ultrasonic techniques. *Ndt & E International*, 67, 10–16.
- Chen, J., Yin, T., Kim, J. Y., Xu, Z., & Yao, Y. (2017). Characterization of thermal damage in sandstone using the second harmonic generation of standing waves. *International Journal of Rock Mechanics and Mining Sciences*, 91, 81–89.
- Climent, M. A., de Vera, G., Viqueira, E., & López-Atalaya, M. M. (2004). Generalization of the possibility of eliminating the filtration step in the determination of acid-soluble chloride content in cement and concrete by potentiometric titration. *Cement and Concrete Research*, 34(12), 2291–2295.
- Climent, M. Á., Miró, M., Carbajo, J., Poveda, P., de Vera, G., & Ramis, J. (2019). Use of non-linear ultrasonic techniques to detect cracks due to steel corrosion in reinforced concrete structures. *Materials*, 12, 813.
- Climent, M. A., Sánchez de Rojas, M. J., de Vera, G., & Garcés, P. (2006). Effect of type of anodic arrangements on efficiency of electrochemical chloride removal from concrete. *ACI Materials Journal*, 103(4), 243.
- Climent, M. A., Viqueira, E., de Vera, G., & López, M. M. (1998). Chloride contamination of concrete by interaction with PVC combustion gases. *Cement and Concrete Research*, 28(2), 209–219.
- Dakel, 2019, *Last consulted: December 2019, IDK09*, <http://www.dakel.cz>.
- EHE-08, 2010, *Instrucción de Hormigón Estructural* (Spanish Structural Concrete Code): Ministerio de Fomento, Madrid, Spain. (In Spanish)
- Elsener, B., Andrade, C., Gulikers, J., Polder, R., & Raupach, M. (2003). Recommendation on half-cell potential measurements. *Materials and Structures*, 36, 461–471.
- Farina, A., 2000, Simultaneous measurement of impulse response and distortion with a swept-sine technique. In: *Audio Engineering Society Convention 108*, Audio Engineering Society.
- Friswell, M. I., & Penny, J. E. (2002). Crack modeling for structural health monitoring. *Structural Health Monitoring—an International Journal*, 1, 139–148.
- Jhang, K. Y. (2000). Applications of nonlinear ultrasonics to the NDE of material degradation. *IEEE Transactions on Ultrasonics, Ferroelectrics, and Frequency Control*, 47(3), 540–548.
- Jhang, K. Y. (2009). Nonlinear ultrasonic techniques for nondestructive assessment of micro damage in material: a review. *International Journal of Precision Engineering and Manufacturing*, 10, 123–135.
- Kim, G., Loreto, G., Kim, J. Y., Kurtis, K. E., Wall, J. J., & Jacobs, L. J. (2018). In situ nonlinear ultrasonic technique for monitoring microcracking in concrete subjected to creep and cyclic loading. *Ultrasonics*, 88, 64–71.
- Klippel, W. (2006). Tutorial: loudspeaker nonlinearities—causes, parameters, symptoms. *Journal of the Audio Engineering Society*, 54, 907–939.
- Korenska, M., Matysik M., Vyrubal P., & Pospisil K., 2009, Assessment of reinforcement corrosion using nonlinear ultrasonic spectroscopy. In: *Proceedings of the 5th NDT Progress—International Workshop of NDT Experts*, Prague, Czech Republic.
- Kwun, H., Burkhardt G. L., & Fisher J. L., 1993, Detection of reinforcing steel corrosion in concrete structures using non-linear harmonic and intermodulation wave generation, Google Patents.
- Laureti, S., Ricci, M., Mohamed, M. N., Senni, L., Davis, L. A., & Hutchins, D. A. (2018). Detection of rebars in concrete using advanced ultrasonic pulse compression techniques. *Ultrasonics*, 85, 31–38.
- Liang, M. T., & Su, P. J. (2001). Detection of the corrosion damage of rebar in concrete using impact-echo method. *Cement and Concrete Research*, 31, 1427–1436.
- Mohamed, M. N. I. B., Laureti, S., Davis L. A. J., Hutchins D. A., Ricci M. & Burrascano P., 2015, Low frequency coded waveform for the inspection of concrete structures. In: *2015 IEEE International Ultrasonics Symposium (IUS)*, p. 1–4, IEEE.
- Molina, F. J., Alonso, C., & Andrade, C. (1993). Cover cracking as a function of rebar corrosion. 2. *Numerical Model: Materials and Structures*, 26, 532–548.
- Muller, M., Sutin, A., Guyer, R., Talmant, M., Laugier, P., & Johnson, P. A. (2005). Nonlinear resonant ultrasound spectroscopy (NRUS) applied to damage assessment in bone. *Journal of the Acoustical Society of America*, 118, 3946–3952.
- Nossoni, G., & Harichandran, R. (2012). Current efficiency in accelerated corrosion testing of concrete. *Corrosion (NACE)*, 68, 801–809.
- Novak, A., Lotton, P., & Simon, L. (2015). Synchronized swept-sine: theory, application, and implementation. *Journal of the Audio Engineering Society*, 63(10), 786–798.
- Novak, A., Simon, L., Kadlec, F., & Lotton, P. (2010). Nonlinear system identification using exponential swept-sine signal. *IEEE Transactions on Instrumentation and Measurement*, 59(8), 2220–2229.
- Ohtsu, M. (2010). Recommendation of RILEM TC 212-ACD: acoustic emission and related NDE techniques for crack detection and damage evaluation in concrete. *Materials and Structures*, 43, 1177–1189.
- Payan, C., Garnier, V., & Moysan, J. (2010). Effect of water saturation and porosity on the nonlinear elastic response of concrete. *Cement and Concrete Research*, 40(3), 473–476.
- Pedrosa, F., & Andrade, C. (2017). Corrosion induced cracking: effect of different corrosion rates on crack width evolution. *Construction and Building Materials*, 133, 525–533.
- Price J., & Goble T., 1993, Signals and noise. In: *Telecommunications Engineer's Reference Book* (Editor F. F. Mazda), Chapter 10, Butterworth-Heinemann Ltd., Oxford, UK.
- Raichel, D. R. (2006). *The science and applications of acoustics (AIP Series in Modern Acoustics and Signal Processing)* (pp. 625–626). New York: Springer.
- Scalcerandi, M., Gliozi, A. S., Bruno, C. L. E., Masera, D., & Bocca, P. (2008). A scaling method to enhance detection of a nonlinear elastic response. *Applied Physics Letters*, 92(10), 101912.

- Shah, A. A., & Ribakov, Y. (2009a). Non-destructive evaluation of concrete in damaged and undamaged states. *Materials and Design*, 30, 3504–3511.
- Shah, A. A., & Ribakov, Y. (2009b). Non-linear ultrasonic evaluation of damaged concrete based on higher order harmonic generation. *Materials & Design*, 30, 4095–4102.
- Van den Abeele, K. E. A., Carmeliet, J., Ten Cate, J. A., & Johnson, P. A. (2000). Nonlinear elastic wave spectroscopy (NEWS) techniques to discern material damage, Part II: Single-mode nonlinear resonance acoustic spectroscopy. *Research in Nondestructive Evaluation*, 12, 31–42.
- Woodward, C. and M. N. Amin, 2008, Evaluating rebar corrosion using nonlinear ultrasound. In: *AIP Conference Proceedings*, American Institute of Physics: College Park, v. 975, p. 1314–1319.
- Zaki, A., Chai, H. K., Aggelis, D. G., & Alver, N. (2015). Non-destructive evaluation for corrosion monitoring in concrete. A review and capability of acoustic emission technique. *Sensors*, 15, 19069–19101.

Publisher's Note

Springer Nature remains neutral with regard to jurisdictional claims in published maps and institutional affiliations.

Submit your manuscript to a SpringerOpen® journal and benefit from:

- Convenient online submission
- Rigorous peer review
- Open access: articles freely available online
- High visibility within the field
- Retaining the copyright to your article

Submit your next manuscript at ► springeropen.com
